Vector control strategies for synchronous reluctance motor: constant current control, MTPA, MTPW and MPFC

Yassine Zahraoui, Mohamed Moutchou, Souad Tayane

Vector control strategies for synchronous reluctance motor: constant current control, MTPA, MTPW and MPFC

Yassine Zahraoui*, Mohamed Moutchou and Souad Tayane

Department of Electrical Engineering,
Laboratory of Complex Cyber-Physical Systems (LCCPS),
Higher National School of Arts and Crafts (ENSAM),
Hassan II University,
Casablanca 20670, Morocco
Email: yassine.zahraoui1-etu@etu.univh2c.ma
Email: mohamed.moutchou@univh2c.ma
Email: souad.tayane@univh2c.ma
*Corresponding author

Abstract: This paper presents different vector control strategies in order to improve the performance of a synchronous reluctance motor. As the torque control is directly related to the current control, many strategies can be implemented. Depending on the criterion to be optimised, there are therefore many strategies. The suitable control strategy choice is mainly determined by the way the current reference values will be defined. For that purpose, four techniques are detailed: constant current control, maximum torque per Ampere; maximum torque per Weber, and maximum power factor control. All these techniques have been simulated in MATLAB/Simulink, and precise comparison of their characteristics is brought out. The obtained results are satisfactory and good performance is achieved, such as response time, torque ripples reduction, and current improvement. These results will help in deciding which of the four-vector control strategies can be employed in high-performance drive applications, and when and under what conditions.

Keywords: synchronous reluctance motor; vector control strategies; constant direct current control; constant current angle control; maximum torque per ampere; MTPA; maximum torque per Weber; MTPW; maximum power factor control; MPFC; ripples reduction.

Reference to this paper should be made as follows: Zahraoui, Y., Moutchou, M. and Tayane, S. (xxxx) 'Vector control strategies for synchronous reluctance motor: constant current control, MTPA, MTPW and MPFC', *Int. J. Modelling, Identification and Control*, Vol. x, No. x, pp.xxx–xxx.

Biographical notes: Yassine Zahraoui earned a Master's in Data Processing from Hassan II University, Casablanca in 2011. He received his PhD in Electrical Engineering from Mohammed V University, Mohammadia School of Engineering (EMI), Rabat in 2021. He is currently a PhD student for a second thesis at the University of Hassan II, Higher National School of Arts and Crafts (ENSAM), Casablanca. His research interests include the AC drives robust and sensorless control strategies, especially synchronous reluctance and induction motors. His main research focuses on ripple reduction and performance improvement. Future prospects are focused on electric cars and renewable and sustainable energy sources.

Mohamed Moutchou received his PhD in Electrical Engineering from Mohammed V University, Mohammadia School of Engineering (EMI), Rabat, in 2015. Since 2016, he has been a Professor of Electrical Engineering at the Higher National School of Arts and Crafts (ENSAM), Casablanca, where he continued developing his research on DC and AC electrical drives and control, and photovoltaic/wind energy renewable sources. His recent research interests are energy quality, energy recovery for the IoT and Industry 4.0. He is responsible for the Laboratory of Electronic Components and Conception in ENSAM, Casablanca. Since 2017, he has been the General Secretary of the Association of Connected Objects and Smart Systems, domiciled at ENSAM. Since 2022, he has been an Associate Director of the Research Laboratory of Complex Cyber-Physical Systems and a permanent member of the Research Team for Smart Control, Diagnostic, and Renewable Energy.

Souad Tayane received her PhD in Physical Chemistry from Hassan II University, Casablanca, in 2000. Currently, she is a Professor of Industrial Chemistry and Project Management at the Higher National School of Arts and Crafts (ENSAM), Casablanca, where she develops research on smart materials, bio-based materials, and biomaterials. Prior to joining ENSAM

of Casablanca, she was a Research Scientist at the Laboratory of Catalytic Reactivity Studies of Surfaces and Interfaces at Louis Pasteur University, Strasbourg, France. Her research interests include the development of composite materials, bio-organic materials, bio-materials, and bio-sourced materials and their industrial applications.

1 Introduction

Electrical machines offer many advantages which are accentuated by the development of complementary technologies in power electronics and industrial computing. These advantages lead electric machines to replace the classic solutions offered by thermal motors, mechanics, or hydraulics in many sectors such as industry or transport. Renewable energies also constitute a tremendous opportunity for the development of electrical machines, whether they are slow, in the case of the direct conversion of wind or tidal energy, or on the contrary, very fast to carry out inertial storage, for example. Electric motors consume nearly 60% of total electrical energy in industries. The efficiency of an electric motor is therefore a fundamental parameter. Recently, many authors have proposed different control and powering methods in order to optimise their performance (El-Refaie, 2019).

The synchronous reluctance machine (SynRM) has received much attention for many applications in the industry in recent years due to its simple structure and low manufacturing cost. The SynRM is also functionally robust; it is relatively well working as it has no associated permanent magnets, which is also an advantage for high-temperature applications (Zakharov et al., 2018). Therefore, it has no demagnetisation problems or associated losses. In the sensorless control domain, it has a major advantage compared to an induction machine because it has a natural salience. In addition, there are no rotor losses, which allows a higher mass torque than that of an induction machine. These different advantages seem to give it chance for new developments (Murataliyev et al., 2022).

However, SynRm has also significant drawbacks. The salience of the rotor which is at the origin of the electromagnetic torque causes ripples on the latter, which can result in vibrations and acoustic noise. The power factor of this type of machine is generally low leading to over-sizing of the inverter (Kim et al., 2020). In addition, it is very sensitive to magnetic saturation, which has a strong impact on the developed average torque. The main objective of this work is to develop vector control optimisation methods in order to increase the performance of the SynRM, especially in terms of efficiency (Babetto et al., 2018).

Because of the limitations of reached current and stator voltage according to the used strategy, many criteria can be favoured. For example, minimising the current for a given torque to reduce the Joule losses [a method known as maximum torque per ampere – MTPA (Accetta et al., 2020)] and minimising the current for a given torque to reduce the power factor [a method known as maximum power factor control – MPFC (Chen et al., 2021)].

Developing optimisation methods at the control level in order to increase SynRM performance remains a hot topic, as shown by a large number of recent publications. The current applications of the SynRM are in the fields of the textile industry, machine tools, and applications with high rotational speeds. Recently, it has been used for traction, electric vehicle, pumping, and ventilation applications (Gallicchio et al., 2022; Yamashita and Okamoto, 2020).

This research paper aims to improve the performance of SynRM vector control by proposing four robust techniques. The research can be summarised in two stages:

- the vector control is improved by exploiting a degree of freedom which helps to optimise efficiency, speed range and power factor
- there are therefore as many control strategies as criteria, and the most interesting strategies have been highlighted and explained.

2 SynRM state-space mathematical model

The variable speed control of the synchronous reluctance motor requires the knowledge of its dynamic model defined by the electrical and mechanical parameters, which describe the electromagnetic and electromechanical phenomena. According to Arafat and Choi (2018) and Carlet et al. (2019), the classical model based on the Park transformation respects the following assumptions:

- the hysteresis in the magnetic circuits is negligible
- the magnetic circuit is unsaturated
- gap harmonics are not taken into account
- the spatial distribution of the magneto-motive forces in the air gap is sinusoidal
- the effect of temperature on the value of resistors is neglected.

The electrical equations of the SynRM in the d-q reference frame are:

$$\begin{bmatrix} v_{ds} \\ v_{qs} \end{bmatrix} = R_s \begin{bmatrix} i_{ds} \\ i_{qs} \end{bmatrix} + \begin{bmatrix} L_d \\ L_q \end{bmatrix} \frac{d}{dt} \begin{bmatrix} i_{ds} \\ i_{qs} \end{bmatrix} + p\Omega \begin{bmatrix} 0 & -L_q \\ L_d & 0 \end{bmatrix} \begin{bmatrix} i_{ds} \\ i_{qs} \end{bmatrix} \quad (1)$$

i_{ds} and i_{qs} are current components in the d-q reference frame. v_{ds} and v_{qs} are stator voltage components. R_s is the stator resistance. L_d and L_q are the inductance of the direct and the quadrature axis. Ω is the mechanical speed and p is the pole pair number. The electromagnetic torque is expressed as:

$$T_{em} = \frac{3}{2} p (L_d - L_q) i_{ds} i_{qs} \quad (2)$$

Figure 1 Steady-state vector diagram of the SynRM

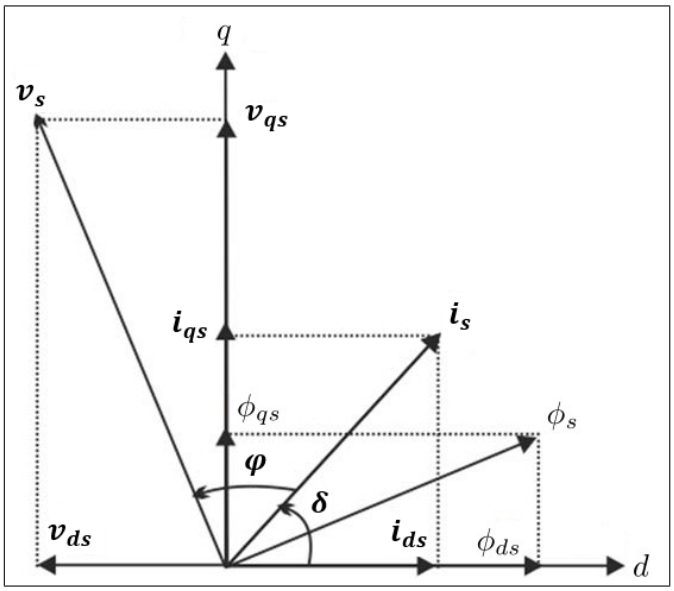

Table 1 Rated power and parameters of the SynRM

Rated power	1.1 kW
Rated speed	1,500 tr/min
Rated voltage	220/380 V
Rated torque	7 N.m
Frequency	50 Hz
Pole pair	2
Stator resistance	6.2 Ω
Apparent stator inductance L_d	0.34 H
Apparent stator inductance L_q	0.105 H
Inertia moment	0.008 N.m.s^2
Viscous friction coefficient	0.0001 N.m.s/rad

In the frame related to the rotor, the total flux through the windings d and q is expressed by:

$$\begin{cases} \phi_{ds} = L_d i_{ds} \\ \phi_{qs} = L_q i_{qs} \end{cases} \tag{3}$$

hence

$$\begin{cases} v_{ds} = R_s i_{ds} + \frac{d\phi_{ds}}{dt} - p\Omega\phi_{qs} \\ v_{qs} = R_s i_{qs} + \frac{d\phi_{qs}}{dt} + p\Omega\phi_{ds} \end{cases} \tag{4}$$

with

$$\phi_s = \sqrt{\phi_{ds}^2 + \phi_{qs}^2} \tag{5}$$

and

$$\tan\delta = \frac{i_{qs}}{i_{ds}} \tag{6}$$

The torque equation in (2) becomes:

$$T_{em} = p(\phi_{ds} i_{qs} - \phi_{qs} i_{ds}) \tag{7}$$

and the rotor motion is expressed by:

$$J\frac{\Omega}{dt} = T_{em} - T_L - f\Omega \tag{8}$$

where J is the motor inertia, T_L is the load torque, and f is the friction coefficient. The synchronous reluctance motor model in (1) is nonlinear; the terms of nonlinearity are the product between the current and the mechanical speed on one hand, and between the current and its derivative on the other hand (Heidari et al., 2021; Noussi et al., 2021). Figure 1 shows the vector diagram of the synchronous reluctance motor in the steady-state.

The rated parameters of the machine used in the simulation are listed in Table 1.

3 Vector control of SynRM

Controlling the SynRM torque means indirectly controlling the i_{ds} and i_{qs} stator current components in the d-q reference frame. However, as the torque is proportional to product $i_{ds}.i_{qs}$, a degree of freedom allows optimising an additional criterion (efficiency, speed range, power factor, etc.). There are therefore as many control strategies as criteria. The vector control law has two current loops (one for each axis) and a loop for speed regulation (Ismaeel et al., 2019; Zerzeri and Khedher, 2021).

3.1 Vector control architecture

The block diagram of the SynRM vector control architecture is presented in Figure 2. The asterisk * designates the reference quantities. This cascade structure is classic and has three levels of control. The first level corresponds to the current loops. These loops control the stator current d-q components, in order to achieve constant signals in the steady-state. A simple PI controller guarantees then zero static error and rejects the electromotive force which couples the two axes (d and q) (Zahraoui et al., 2019).

The second level defines the current set-points i_{ds}^* and i_{qs}^* depending on the desired torque. The goal is to optimise current and voltage limitations. Finally, the last level concerns speed control and use differently an IP controller (Zahraoui et al., 2020). The PI controllers tuning gains have been calculated by pole placement technique (Zahraoui et al., 2022).

3.2 Vector control strategies

From the torque equation of the SynRM defined in equation (2), it is clear that the control of the electromagnetic torque is based on controlling the currents i_{ds} and i_{qs} simultaneously, giving an additional degree of freedom. The choice of control strategy will depend on how to define the i_{ds}^* and i_{qs}^* references. Several strategies exist and are differentiated by the criterion to be optimised (maximising torque, efficiency, or power factor) and the required performance (for example, torque control at low speed or during transients, etc.) (Dwivedi et al., 2020).

Figure 2 Vector control structure of the synchronous reluctance motor

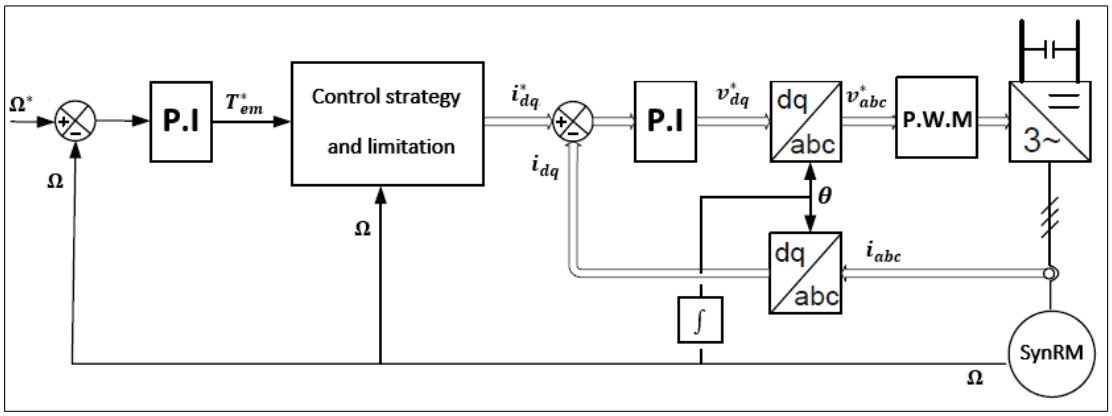

3.3 Constant current control

When the required speed control Ω is less than the nominal value Ω_n, then this vector control type is suitable for this case. Below nominal speed, i_{ds} current component is kept constant (Scalcon et al., 2021), hence:

$$i_{ds}^{*} = C^{te} \tag{9}$$

where

$$C^{te} = \frac{\phi_{s_{max}}^{*}}{L_d\sqrt{2}} \tag{10}$$

Stator flux-linkage maximum value is then derived from the electromagnetic torque reference value:

$$\phi_{s_{max}}^{*} = \sqrt{\frac{4T_{em}^{*}L_dL_q}{3p(L_d - L_q)}} \tag{11}$$

Above nominal speed, i_{ds} current component decreases with speed as follow:

$$i_{ds}^{*} = \frac{\Omega_n}{\Omega}C^{te} \tag{12}$$

The q-stator current reference, based on equation (2), is obtained as:

$$i_{qs}^{*} = \frac{T_{em}^{*}}{3p(L_d - L_q)i_{ds}^{*}} \tag{13}$$

3.4 Constant current angle control

There are three different strategies of constant current angle control. These strategies are *MTPA*, *MTPW* and *MPFC*. The d and q-axis reference currents are estimated from the reference value of torque utilising the values of the tangent of the current angle (δ), which is the angle between the current space vector and rotor-oriented d-axis stator current. A brief description about estimation of reference currents is included below for different current angle control techniques (Lin et al., 2020).

Figure 3 MTPA control trajectory (see online version for colours)

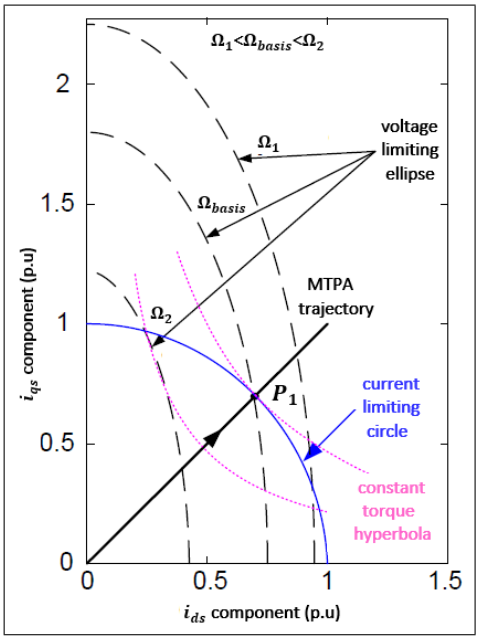

3.4.1 MTPA strategy

This strategy is used mainly at start-ups and for low speed (Tinazzi et al., 2019). The electromagnetic torque can be expressed by:

$$\begin{aligned} T_{em} &= \frac{3}{2}p(L_d - L_q)i_{ds}i_{qs} \\ &= \frac{3}{2}p(L_d - L_q)i_s^2\sin(2\delta) \end{aligned} \tag{14}$$

For a fixed current modulus i_s, the maximum torque in absolute value is obtained for $\delta = \pm\frac{\pi}{4}$. We then obtain $i_{ds} = |i_{qs}|$, hence the references of the currents:

$$i_{ds}^{*} = \frac{2T_{em}^{*}}{3p(L_d - L_q)} \tag{15}$$

and

$$i_{qs}^{*} = i_{ds}^{*}sign(T_{em}^{*}) \tag{16}$$

When the current starts to increase, it follows a 45° direction starting from point O to reach the current limit $i_{ds_{max}}$ at point P_1 (Figure 3) corresponding to the maximum torque.

3.4.2 MTPW strategy

The MTPW or maximum torque per volt (MTPV) strategy is used when the MTPA method does not ensure high performance, the cause is the voltage limitation due to the increase in speed. In steady-state, the stator voltage is proportional to the stator flux and the rotational speed: $v_d \propto \phi_s \Omega$. Therefore, for a given speed and limiting voltage, the corresponding stator flux can be determined (Mahmoud et al., 2018). The maximum torque per flux unit (MTPW) strategy consists in choosing $\delta = \pm\frac{\pi}{4}$ (Figure 4), what leads to the following current references form:

$$i_{ds}^* = \frac{2L_q T_{em}^*}{3pL_d(L_d - L_q)} \tag{17}$$

and

$$i_{qs}^* = \frac{L_d}{L_q} i_{ds}^* sign(T_{em}^*) \tag{18}$$

3.4.3 MPFC strategy

The MPFC or maximum torque per kilo-volt-ampere (MTPkVA) strategy is used to supplement certain operating conditions, so as not to have to oversize the static converter (Sangwongwanich, 2020). The power factor can be obtained from the following expression:

$$f_p = \frac{v_{ds} i_{ds} + v_{qs} i_{qs}}{|v_s||i_s|} \tag{19}$$

hence

$$f_p = cos(\phi) = (\xi - 1)\sqrt{\frac{\sin(2\delta)}{2\tan(\delta) + \xi^2 \text{cotan}(\delta)}} \tag{20}$$

The power factor $f_p = f_\delta$ is given by a curve (Figure 5) which has a maximum which is $\frac{\xi-1}{\xi+1}$ for the angle δ such that $\tan(\delta) = \sqrt{\xi}$. To obtain a good power factor, a large salience ratio is therefore required, which justifies the flux barrier or axially laminated rotors.

3.4.4 Synthesis of strategies

In Figure 5, the possible operating points are represented from point A to G. Point A corresponds to the MTPA strategy, point G corresponds to the MPFC strategy and point C corresponds to the MTPW strategy. These three points produce the same torque for different current values (Kerdsup et al., 2018). Points A, D, and B have the same current but different fluxes and different power factors.

If the MTPA strategy is used at a low speed, switching to the other points is necessary if the speed increases sufficiently. In the method proposed by some authors (Cheng and Tsai, 2021; Lee et al., 2022), the trajectory is from point A to point D (point giving the maximum power factor MPFC for $\tan(\delta) = \sqrt{\xi}$).

Figure 4 MTPW control trajectory (see online version for colours)

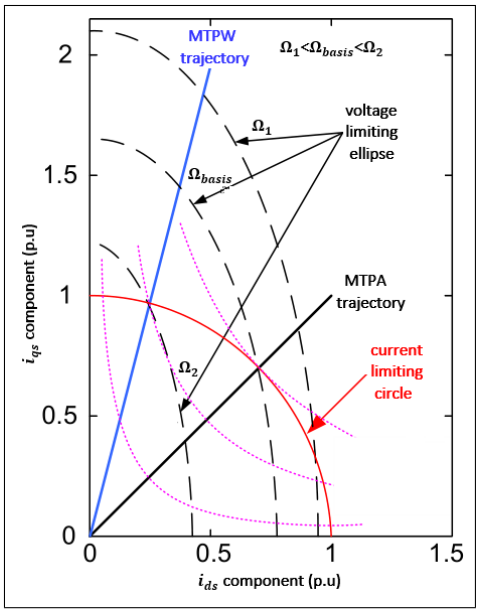

Another trajectory is proposed to switch from the MTPA method, which is always used at start-up and at low speed, to the MPFC method when limitations appear. In this method, an angle $\delta = 45°$ for which $i_{ds} = i_{qs}$ must be imposed first, and when the speed increases this strategy can no longer be maintained because the flux on the d-axis cannot exceed the nominal value of the stator flux: $i_{ds_{max}} x_d = \Omega \phi_{s_{max}}$. When the current on the d-axis reaches its maximum value $i_{ds_{max}}$, $i_{ds} = i_{ds_{max}}$ is kept and i_{qs} is varied, such that:

$$i_{qs}^* = \frac{2T_{em}}{3p(L_d - L_q) i_{ds_{max}}} \tag{21}$$

The objective is to arrive at the MTPW method where $\tan(\delta) = \frac{i_{ds}}{i_{qs}} = \sqrt{\xi} = \sqrt{\frac{L_d}{L_q}}$.

3.5 Control setting

3.5.1 Choice of sampling period

To obtain efficient vector control for a synchronous reluctance machine, it is important to choose a sufficiently small sampling period. In fact, the reference voltages calculated by the control law will be blocked and therefore constant during this period. However, in the steady state, the phase of the stator voltages must evolve all the more quickly as the machine rotates at high speed (Lin et al., 2019; Varatharajan et al., 2022). For an angular velocity Ω, during a sampling period T_s, the rotor of the machine rotates through an angle:

$$\Delta\theta = \Omega T_s \tag{22}$$

Figure 5 Network of curves giving power factor and torque with stator flux and stator current as parameters (see online version for colours)

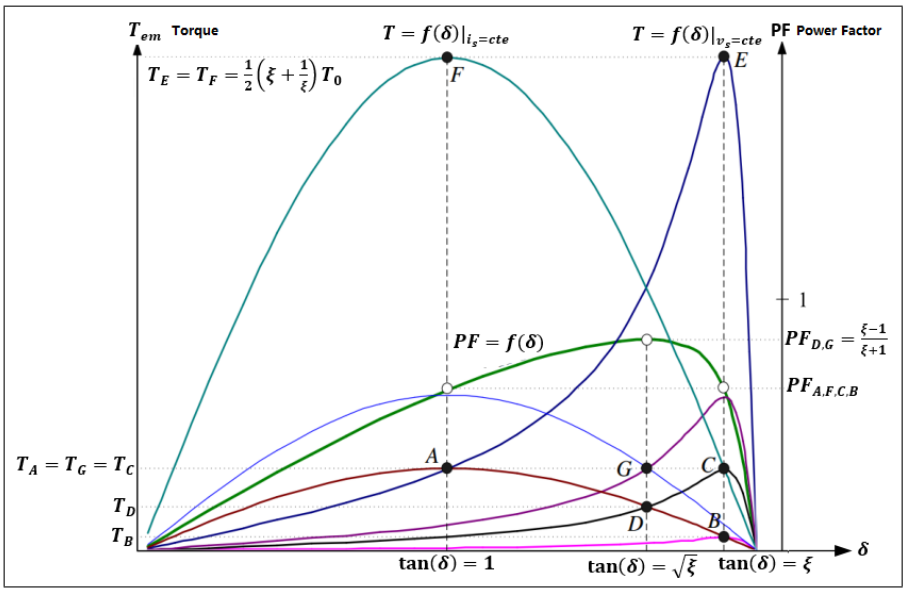

Figure 6 Test of performance comparison under load torque disturbance, (a) test at 100 rad/s speed step with load application (b) test at 100 rad/s reverse speed step with load application (see online version for colours)

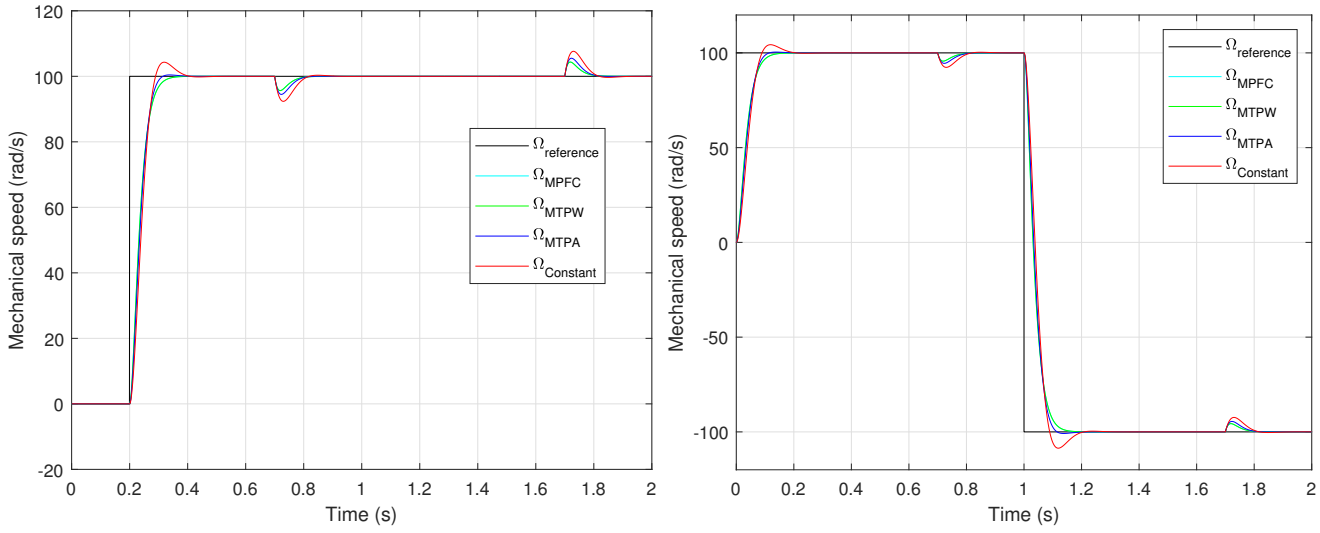

In steady-state, the phase of the reference voltages changes only because of the Park transformation which is related to the position of the rotor. It must therefore be updated at period T_s. For sensorless control, this may cause computing power problems.

3.5.2 *Choice of stator current dynamics*

The instantaneous torque of the SynRM is proportional to the product of the i_{ds} and i_{qs} stator current components. The previous section presented the different solutions allowing to take advantage of this degree of freedom in the steady state. It remains to consider the management of transitional regimes.

The behaviour of the SynRM could resemble to that of a DC machine with separate excitation, if the dynamics of the current i_{ds} were much lower than that of the current i_{qs}. However, unlike other machines for which the inductor has a high inductance, the inductance L_d and L_q of the SynRM are of the same order of magnitude so the dynamic performance of the current loops of the d and q axes are also close.

The tests showed that it was necessary to slow down the dynamics of the current i_{ds}, otherwise, the current i_{qs} could not follow its reference when the speed is high. The problem arises in particular when switching from MTPA mode to MTPW mode which generates a rapid change in the set-points i_{ds} and i_{qs}. We then observe that the term $L_d \frac{di_{ds}}{dt}$ saturates the inverter in voltage, to the detriment of the current i_{qs} which cannot reach its reference.

Figure 7 Speed error between the four strategies, (a) speed error: $\Omega_{reference} - \Omega_{MPFC}$ (b) speed error: $\Omega_{MPFC} - \Omega_{MTPW}$ (c) speed error: $\Omega_{MPFC} - \Omega_{MTPA}$ (d) speed error: $\Omega_{MPFC} - \Omega_{Constant}$ (e) speed error: $\Omega_{MTPW} - \Omega_{MTPA}$ (f) speed error: $\Omega_{MTPA} - \Omega_{Constant}$

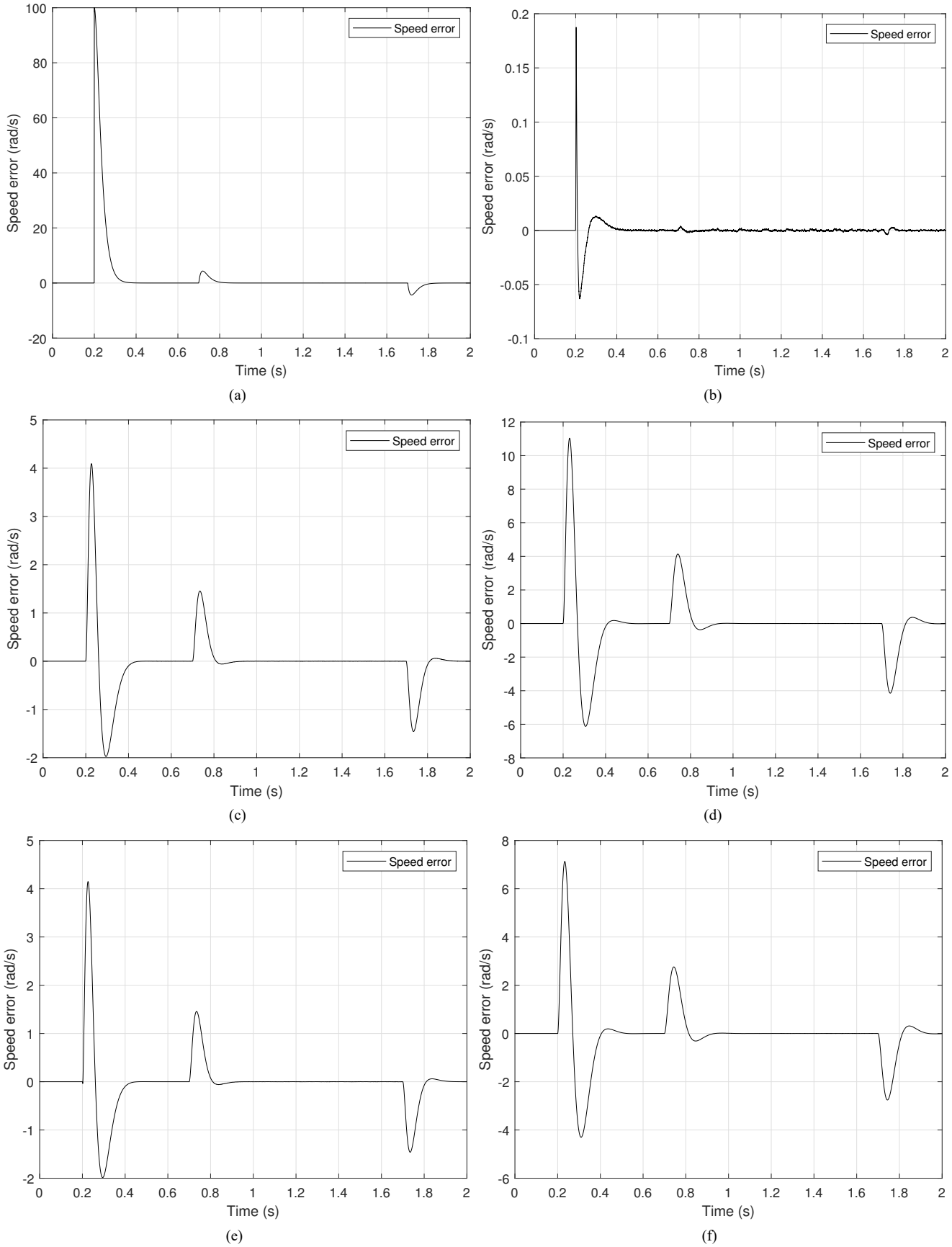

Figure 8 Torque waveform of the four strategies, (a) electromagnetic torque: MPFC (b) electromagnetic torque: MTPW (c) electromagnetic torque: MTPA (d) electromagnetic torque: constant current (see online version for colours)

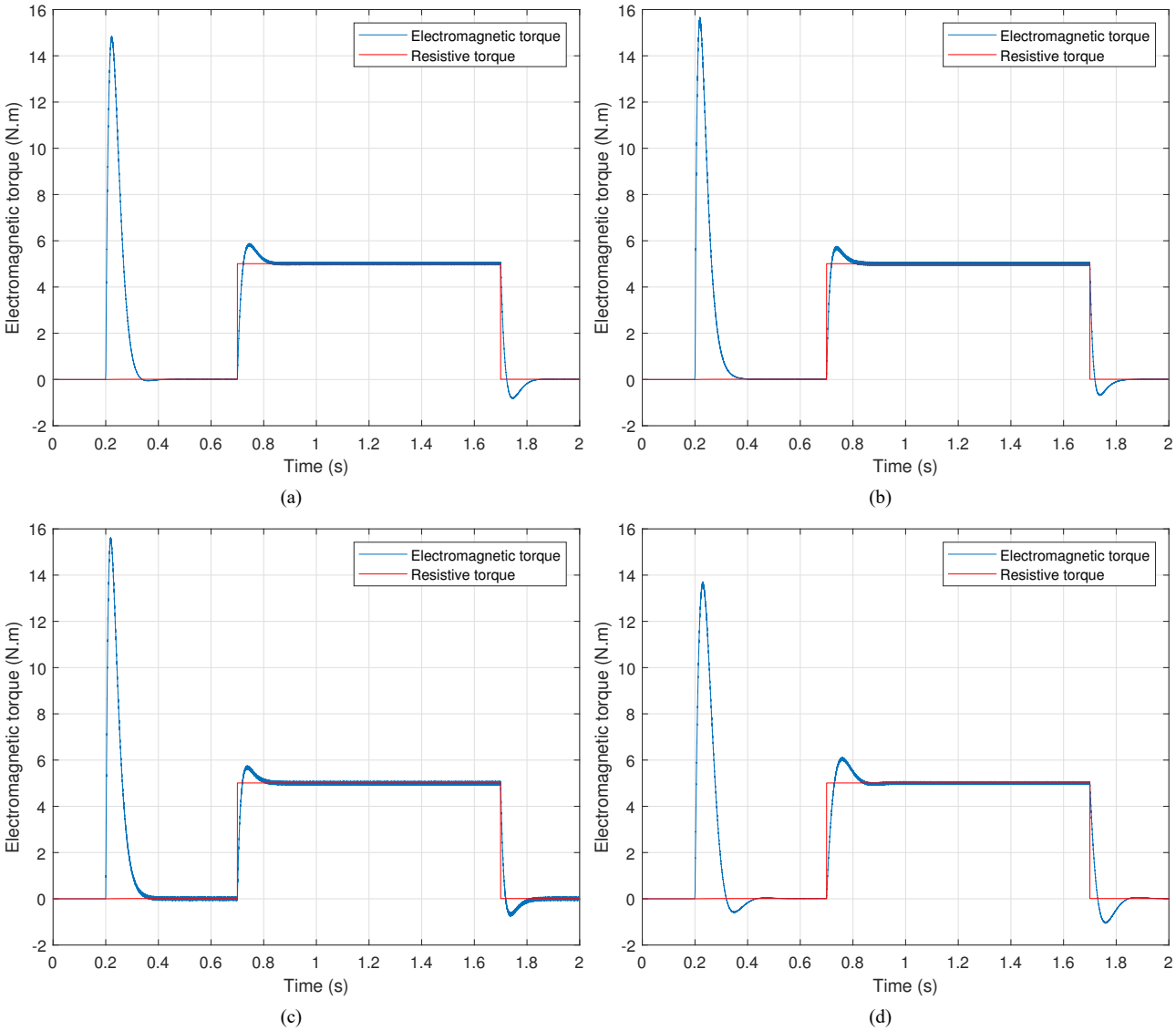

The simplest solution would be to make $i_{ds} = C^{te}$, to the detriment of the performance of the machine. But, we would then lose one of the advantages of synchronous reluctance machine, compared to synchronous permanent magnet machine. We will therefore keep the MTPA command which varies i_{ds}, but decreases its dynamics, compared to that of i_{qs}. Experimental tests have shown that it takes at least a ratio of ten between these two dynamics. This is achieved by adding low-pass filtering of the i_{ds} reference. The dynamics of the torque will therefore be given by that of the current i_{qs} (Li et al., 2019; Tawfiq et al., 2021).

4 Results and discussion

4.1 Simulation environment

The block diagram of the synchronous reluctance motor closed-loop vector control is shown in Figure 2. The rated power and parameters of the machine used in simulation are given in Table 1. The same speed and current controllers have been used for all four techniques (constant current, MTPA, MTPW, and MPFC).

Figure 6 shows the mechanical speed response at a speed step of 100 rad/s and at reverse speed. To demonstrate the robustness of these control methods throughout the steady-state phase, a load torque of 5 N.m is introduced at $t_1 = 0.7$ s and removed at $t_2 = 1.7$ s. Figure 7 displays the speed error between the different techniques. Figure 8 exposes the electromagnetic torque waveform. While Figure 9 shows the phase current waveform. Figure 10 displays the d-q current components waveform.

Figure 9 Phase current waveform of the four strategies, (a) phase current: MPFC (b) phase current: MTPW (c) phase current: MTPA (d) phase current: constant current (see online version for colours)

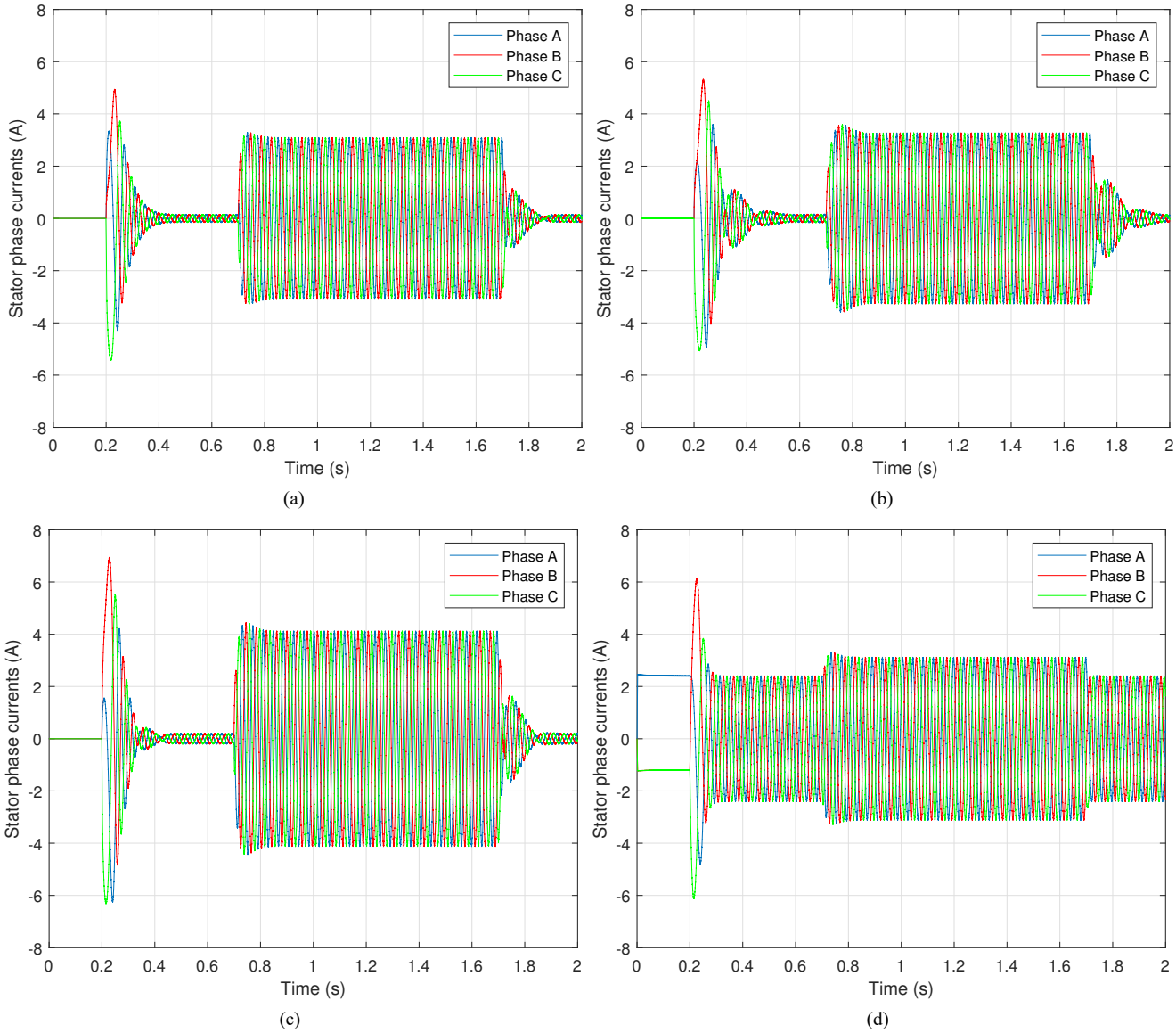

4.2 Results analysis

The time response of MPFC, MTPW, and MTPA strategies is very quick compared to the constant current technique. The latter technique is more affected by the load application. The constant current technique has a significant overshoot of the reference. MPFC and MTPW have almost the same response time, with less speed error between them. That speed error does not exceed 0.2 rad/s. Their speed waveforms are almost identical. Even at reverse speed, the three strategies MPFC, MTPW, and MTPA keep the fast response time and do not overshoot the reference. The static error of all techniques in the steady-state is null, which shows the effectiveness of these control strategies.

The torque waveform of MPFC and MTPW has a reduced level of ripples, while the torque of the MTPA has a chopped waveform. The applied load value is 5 N.m, it is introduced at $t_1 = 0.7$ s and removed at $t_2 = 1.7$ s, it can be clearly seen in the torque waveforms.

The phase current waveform of MPFC and MTPW has a reduced magnitude and ripples level. The constant current technique has the highest current consumption rate among all the four strategies.

The d-q current components of MPFC have almost an identical waveform with less magnitude at start-up. The constant current technique and MTPA have the highest magnitude among all the four strategies.

Figure 10 *d-q* current components waveform of the four strategies, (a) *d-q* current components: MPFC (b) *d-q* current components: MTPW (c) *d-q* current components: MTPA (d) *d-q* current components: constant current (see online version for colours)

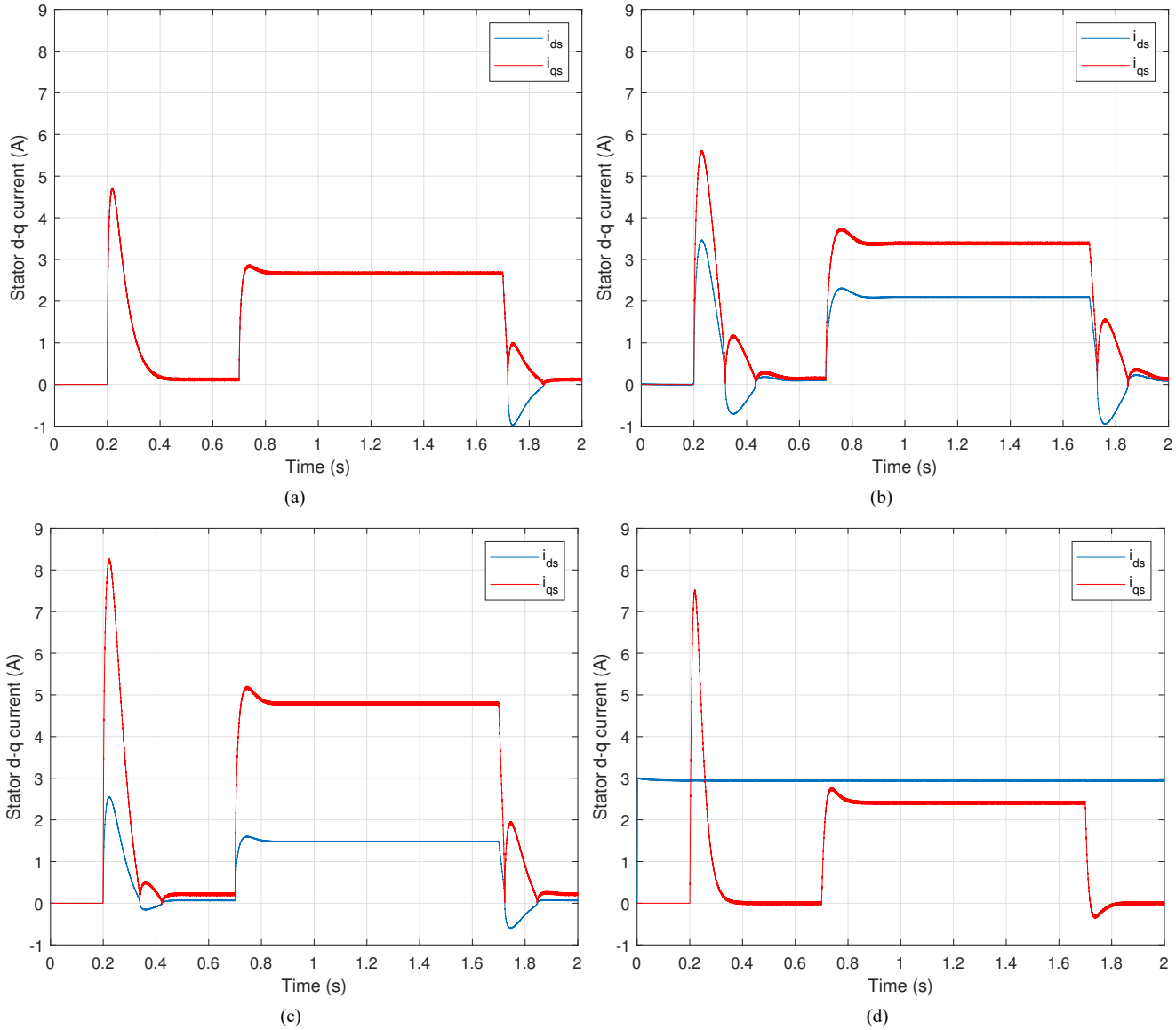

5 Conclusions

In this paper, we presented the modelling, identification, and simulation of many vector control strategies for SynRM operation improvement. The four proposed control strategies offer a degree of freedom in the choice of stator currents since only their product is imposed by the desired torque. Different strategies are then possible, depending on the targeted performance. At low speed and to obtain maximum acceleration and efficiency, the MTPA strategy is generally used. To achieve higher speeds, without requiring the too high voltage of the inverter DC bus, it is then necessary to switch to the MTPW strategy. MPFC strategy is the best because it ensures fewer torque ripples. These vector control strategies have been adjusted, tested, and validated in simulation.

This research can be improved into a robust sensorless scheme. Firstly, the insertion of fuzzy logic controllers instead of PI controllers can be a big deal. Secondly, an extended Kalman filter for mechanical speed observation can replace the speed trans-coder.

References

Accetta, A., Cirrincione, M., Piazza, M.C.D., Tona, G.L., Luna, M. and Pucci, M. (2020) 'Analytical formulation of a maximum torque per ampere (MTPA) technique for SynRMs considering the magnetic saturation', *IEEE Transactions on Industry Applications*, Vol. 56, No. 4, pp.3846–3854.

Arafat, A.K.M. and Choi, S. (2018) 'State space modeling and feedback control of five-phase permanent magnet assisted synchronous reluctance motor under open phase faults', *2018 IEEE Applied Power Electronics Conference and Exposition (APEC)*, pp.1229–1235.

Babetto, C., Bacco, G. and Bianchi, N. (2018) 'Design methodology for high-speed synchronous reluctance machines', *IET Electric Power Applications*, Vol. 12, No. 8, pp.1110–1116.

Carlet, P.G., Tinazzi, F., Bolognani, S. and Zigliotto, M. (2019) 'An effective model-free predictive current control for synchronous reluctance motor drives', *IEEE Transactions on Industry Applications*, Vol. 55, No. 4, pp.3781–3790.

Chen, S-G., Lin, F-J., Liang, C-H. and Liao, C-H. (2021) 'Intelligent maximum power factor searching control using recurrent Chebyshev fuzzy neural network current angle controller for SynRM drive system', *IEEE Transactions on Power Electronics*, Vol. 36, No. 3, pp.3496–3511.

Cheng, L-J. and Tsai, M-C. (2021) 'Robust scalar control of synchronous reluctance motor with optimal efficiency by MTPA control', *IEEE Access*, Vol. 9, pp.32599–32612.

Dwivedi, S., Tripathi, S.M. and Sinha, S.K. (2020) 'Review on control strategies of permanent magnet-assisted synchronous reluctance motor drive', *2020 International Conference on Power Electronics & IoT Applications in Renewable Energy and its Control (PARC)*, pp.124–128.

El-Refaie, A. (2019) 'Toward a sustainable more electrified future: the role of electrical machines and drives', *IEEE Electrification Magazine*, Vol. 7, No. 1, pp.49–59.

Gallicchio, G., Nardo, M.D., Palmieri, M., Marfoli, A., Degano, M., Gerada, C. and Cupertino, F. (2022) 'High speed synchronous reluctance machines: modeling, design and limits', *IEEE Transactions on Energy Conversion*, Vol. 37, No. 1, pp.585–597.

Heidari, H., Rassõlkin, A., Kallaste, A., Vaimann, T., Andriushchenko, E., Belahcen, A. and Lukichev, D.V. (2021) 'A review of synchronous reluctance motor-drive advancements', *Sustainability*, Vol. 13, No. 2, p.729.

Ismaeel, S.M., Allam, S.M. and Rashad, E.M. (2019) 'Current vector control techniques of five-phase synchronous reluctance motor drive systems', *2019 21st International Middle East Power Systems Conference (MEPCON)*, pp.1180–1185.

Kerdsup, B., Takorabet, N. and Nahidmobarakeh, B. (2018) 'Design of permanent magnet-assisted synchronous reluctance motors with maximum efficiency-power factor and torque per cost', *2018 XIII International Conference on Electrical Machines (ICEM)*, pp.2465–2471.

Kim, H., Park, Y., Oh, S-T., Jang, H., Won, S-H., Chun, Y-D. and Lee, J. (2020) 'A study on the rotor design of line start synchronous reluctance motor for IE4 efficiency and improving power factor', *Energies*, Vol. 13, No. 21, p.5774.

Lee, W., Kim, J., Jang, P. and Nam, K. (2022) 'On-line MTPA control method for synchronous reluctance motor', *IEEE Transactions on Industry Applications*, Vol. 58, No. 1, pp.356–364.

Li, G.J., Zhang, K., Zhu, Z.Q. and Jewell, G.W. (2019) 'Comparative studies of torque performance improvement for different doubly salient synchronous reluctance machines by current harmonic injection', *IEEE Transactions on Energy Conversion*, Vol. 34, No. 2, pp.1094–1104.

Lin, F-J., Huang, M-S., Chen, S-G. and Hsu, C-W. (2019) 'Intelligent maximum torque per ampere tracking control of synchronous reluctance motor using recurrent Legendre fuzzy neural network', *IEEE Transactions on Power Electronics*, Vol. 34, No. 12, pp.12080–12094.

Lin, F-J., Huang, M-S., Chen, S-G., Hsu, C-W. and Liang, C-H. (2020) 'Adaptive backstepping control for synchronous reluctance motor based on intelligent current angle control', *IEEE Transactions on Power Electronics*, Vol. 35, No. 7, pp.7465–7479.

Mahmoud, H., Bacco, G., Degano, M., Bianchi, N. and Gerada, C. (2018) 'Synchronous reluctance motor iron losses: considering machine nonlinearity at MTPA, FW, and MTPV operating conditions', *IEEE Transactions on Energy Conversion*, Vol. 33, No. 3, pp.1402–1410.

Murataliyev, M., Degano, M., Di Nardo, M., Bianchi, N. and Gerada, C. (2022) 'Synchronous reluctance machines: a comprehensive review and technology comparison', *Proceedings of the IEEE*, Vol. 110, No. 3, pp.382–399.

Noussi, K., Abouloifa, A., Katir, H., Lachkar, I. and Otmani, F.E. (2021) 'Towards a global nonlinear control strategy for DFIG-based wind turbine in a high wind energy penetrated system', *International Journal of Modelling, Identification and Control*, Vol. 39, No. 2, pp.172–183.

Sangwongwanich, S. (2020) 'On the equivalent circuit of synchronous reluctance motors based on complex inductance concept', *2020 23rd International Conference on Electrical Machines and Systems (ICEMS)*, pp.1478–1483.

Scalcon, F.P., Osório, C.R.D., Koch, G.G., Gabbi, T.S., Vieira, R.P., Gründling, H.A., Oliveira, R.C.L.F. and Montagner, V.F. (2021) 'Robust control of synchronous reluctance motors by means of linear matrix inequalities', *IEEE Transactions on Energy Conversion*, Vol. 36, No. 2, pp.779–788.

Tawfiq, K.B., Ibrahim, M.N., El-Kholy, E.E. and Sergeant, P. (2021) 'Performance improvement of synchronous reluctance machines – a review research', *IEEE Transactions on Magnetics*, Vol. 57, No. 10, pp.1–11.

Tinazzi, F., Bolognani, S., Calligaro, S., Kumar, P., Petrella, R. and Zigliotto, M. (2019) 'Classification and review of MTPA algorithms for synchronous reluctance and interior permanent magnet motor drives', *2019 21st European Conference on Power Electronics and Applications (EPE '19 ECCE Europe)*, pp.P.1–P.10.

Varatharajan, A., Pellegrino, G. and Armando, E. (2022) 'Direct flux vector control of synchronous motor drives: accurate decoupled control with online adaptive maximum torque per ampere and maximum torque per volts evaluation', *IEEE Transactions on Industrial Electronics*, Vol. 69, No. 2, pp.1235–1243.

Yamashita, Y. and Okamoto, Y. (2020) 'Design optimization of synchronous reluctance motor for reducing iron loss and improving torque characteristics using topology optimization based on the level-set method', *IEEE Transactions on Magnetics*, Vol. 56, No. 3, pp.1–4.

Zahraoui, Y., Akherraz, M., Fahassa, C. and Elbadaoui, S. (2019) 'Robust control of sensorless sliding mode controlled induction motor drive facing a large scale rotor resistance variation', *Proceedings of the 4th International Conference on Smart City Applications, SCA '19*, Association for Computing Machinery, New York, NY, USA, pp.1–6.

Zahraoui, Y., Akherraz, M., Fahassa, C. and Elbadaoui, S. (2020) 'Induction motor harmonic reduction using space vector modulation algorithm', *Bulletin of Electrical Engineering and Informatics*, Vol. 9, No. 2, pp.452–465.

Zahraoui, Y., Moutchou, M. and Tayane, S. (2022) 'Robust vector control of synchronous reluctance motor using space vector modulation algorithm', *2022 3rd International Conference on Digital Age & Technological Advances for Sustainable Development (ICDATA)*, pp.1–11.

Zakharov, A., Malafeev, S. and Dudulin, A. (2018) 'Synchronous reluctance motor: design and experimental research', *2018 X International Conference on Electrical Power Drive Systems (ICEPDS)*, pp.1–4.

Zerzeri, M. and Khedher, A. (2021) 'A sensorless mixed DFIM control strategy based on fuzzy-PI speed controller and current sliding mode controller for electric vehicles', *International Journal of Modelling, Identification and Control*, Vol. 38, Nos. 3–4, pp.271–281.